

An Evaluation of the Robustness of Tract-based Measures of White Matter Integrity

M. Li¹, J. Lin², K. Sakaie², E. Beall², L. Stone², R. Bermel², M. D. Phillips², and M. J. Lowe²

¹Cleveland Clinic, Cleveland, Ohio, United States, ²Cleveland Clinic

Introduction

Track based measures of white matter integrity are increasingly being employed in studies of populations with possible compromised white matter integrity (1). Identifying fiber tracks in populations with diseased white matter has obvious possible confounds. Various methods have been proposed to deal with this, including 1) the use of healthy control-based tracking atlases (2,3) as well as non-tensor based probabilistic tracking methods that are less susceptible to problems from regions of low anisotropy (4). To date, there has been no validation of either method with regard to establishing either 1) robust pathway measures in the case of (1), or 2) unbiased pathway identification in the case of (2). We present here a study based on non-rigid image registration to validate the robustness of establishing comparable pathways in a healthy control population and a population of Multiple Sclerosis (MS) patients.

In the following study, we compare track-based measures produced in MS patients with those produced in healthy controls, matched for age and gender, when using cross-registered tracks generated from either the patient or the control. Our hypothesis is that the track-based measures for patient diffusion data will not significantly differ when using the track generated in the patient or a co-registered track generated in the control.

Methods

DTI and Fiber Tracking: DTI data was collected from 6 subjects consisting of 3 MS patients and 3 healthy controls. Each MS patient has one paired control at similar age and of the same gender. Longitudinal diffusivity(λ_1) and transverse diffusivity(λ_2) and fiber tracking density maps were calculated from DTI data. DTI measurements were performed on a Siemens TIM Trio (Erlangen, Germany) with a standard 12-channel head coil. HARDI data were acquired with a twice-refocused spin echo (5) (TE/TR=102/7700msec, 128x128x48 matrix, FOV=256x256x96mm), 71 b=1000 sec/mm² acquisitions with gradient directions selected by a coulomb repulsion algorithm (6), and 8 b=0 acquisitions at equally spaced intervals. Motion correction was performed using FSL(7). Spherical deconvolution, with regularization optimized by generalized cross validation, was performed in each voxel to estimate fiber orientation (8). Regions of Interest (ROI) were drawn in each of right hemisphere and left hemisphere primary sensorimotor regions. The region was identified using the most highly activated region from an fMRI study of bilateral finger tapping (4). Probabilistic tracking between seed and target regions was performed, with each step determined by rejection sampling (9).

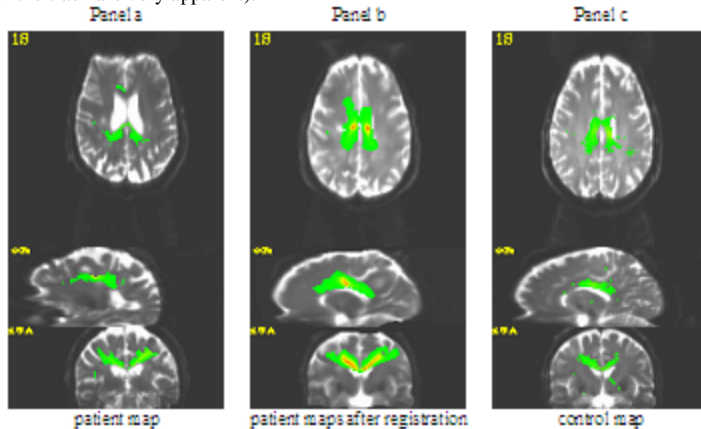
Image/Track Registration: Image registration was carried out in the following steps. 1) DTI b=0 image from each patient was registered to that of the corresponding control. The registration was completed in two steps. In the first step, an affine transformation using FLIRT from FSL toolbox was applied to produce an overall matching between the patient images and control images. In the second step, a multi-resolution non-rigid registration based on b-spline framework from IRTK toolbox (10) was applied on the result of the first step and produce the final registration result. Normalized mutual information metric was used from both steps. 2) The transformations acquired during the registrations in step ii) was applied to track density maps. At this point, we have the track density map of the patient in the frame of the control subjects DTI data set. 3) Register the DTI b=0 and track density maps of control to patient by using the same methods as in step(1) and (2)

Diffusivity computation: Mean longitudinal diffusivity(λ_1) and mean transverse diffusivity(λ_2) for corticospinal tracts are computed in four different combinations: tract density map from control subject and λ_1, λ_2 are also from control subject; tract density map from patient registered to control and λ_1, λ_2 are from control subject; tract density map from patient and λ_1, λ_2 are also from patient; tract density map from control registered to patient and λ_1, λ_2 are from control subject.

Results

1. Registration result of the fiber track density map

In figure 1, panel a-c are corticospinal tract density maps (showing in green color) overlapped on the b=0 images. The result shows that the correspondence of b=0 image between paired patient and control is very high and the geometric features of the track density map are very similar (although differences in the low density parts of the track are very apparent).



2. Mean longitudinal diffusivity(λ_1) and mean transverse diffusivity(λ_2) for corticospinal tracts

In table 1, λ_1 and λ_2 for corticospinal tract are listed. It is apparent that the differences in mean diffusivity value in each case is much less than the standard deviation of the individual measurement. However, the differences between patient-based numbers and control based measures are considerably higher, as is to be expected if the measures are a valid assessment of white matter disease.

Discussion and Conclusion

We present a study of the validity of comparing track-based measures of white matter integrity between a patient population with significant white matter disease and a population of healthy controls. Our method suggests that 1) non-rigid image registration of tracks generated in healthy controls to patient diffusion data and 2) tracking in both patients and controls with a non-tensor based method can result in robust track-based measures of white matter integrity.

Figure 1

Group	Patient λ_1 /Patient Track	Patient λ_1 /Registered Control Track	Patient λ_2 /Patient Track	Patient λ_2 /Registered Control Track	Control λ_1 /Control Track	Control λ_1 /Registered Patient Track	Control λ_2 /Control Track	Control λ_2 /Registered Patient Track
1	1.51±0.723	1.49±0.565	1.07±0.701	0.882±0.527	1.33±0.361	1.32±0.433	0.523±0.207	0.577±0.344
2	1.33±0.457	1.34±0.548	0.523±0.188	0.699±0.457	1.31±0.414	1.38±0.517	0.510±0.187	0.615±0.383
3	1.48±0.452	1.61±0.538	0.822±0.301	1.00±0.523	1.28±0.373	1.37±0.477	0.523±0.183	0.705±0.396

Table 1 (Unit: $\times 10^{-3} \text{ mm}^2/\text{s}$)

References

- Lowe et al., NeuroImage 32:1127-1133 (2006)
- Pagani et al., NeuroImage 26:258-265 (2005)
- Smith et al., NeuroImage 31:1487-1505 (2006)
- Lowe et al., Human Brain Mapping 29:818-827 (2008)
- Reese et al., Magn. Reson. Med. 49:177-182 (2003)
- Jones et al., Magn Reson Med 42:515-525 (1999)
- Smith et al., NeuroImage 23:S208-219 (2004)
- Sakaie et al., NeuroImage 34:169-176 (2007)
- Tournier et al., ISMRM 13:1343 (2005)
- Reuckert et al., IEEE TMI 18:712-721 (1999)